Comparative Kinetics of Cofactor Association and Dissociation for the Human and Trypanosomal *S*-Adenosylhomocysteine Hydrolases. 2. The Role of Helix 18 Stability[†]

Qing-Shan Li,[‡] Sumin Cai,[§] Jianwen Fang,[||] Ronald T. Borchardt,[‡] Krzysztof Kuczera,[§,⊥] C. Russell Middaugh,[‡] and Richard L. Schowen*[,‡,§,⊥]

Departments of Pharmaceutical Chemistry, Chemistry, and Molecular Biosciences and Bioinformatics Core Facility, The University of Kansas, Lawrence, Kansas 66047

Received January 30, 2008; Revised Manuscript Received March 10, 2008

ABSTRACT: The *S*-adenosyl-L-homocysteine (AdoHcy) hydrolases (SAHH) from *Homo sapiens* (Hs-SAHH) and from the parasite *Trypanosoma cruzi* (Tc-SAHH) are very similar in structure and catalytic properties but differ in the kinetics and thermodynamics of association and dissociation of the cofactor NAD^+. The binding of NAD^+ and NADH in SAHH appears structurally to be mediated by helix 18, formed by seven residues near the C-terminus of the adjacent subunit. Helix-propensity estimates indicate decreasing stability of helix 18 in the order Hs-SAHH > Tc-SAHH > Ld-SAHH (from *Leishmania donovani*) > Pf-SAHH (from *Plasmodium falciparum*), which would be consistent with the previous observations. Here we report the properties of Hs-18Pf-SAHH, the human enzyme with plasmodial helix 18, and Tc-18Hs-SAHH, the trypanosomal enzyme with human helix 18. Hs-18Tc-SAHH, the human enzyme with trypanosomal helix 18, was also prepared but differed insignificantly from Hs-SAHH. Association of NAD^+ with Hs-SAHH, Hs-18Pf-SAHH, Tc-18Hs-SAHH, and Tc-SAHH exhibited biphasic kinetics for all enzymes. A thermal maximum in rate, attributed to the onset of local structural alterations in or near the binding site, occurred at 35, 33, 30, and 15 °C, respectively. This order is consistent with some reversible changes within helix 18 but does require influence of other properties of the "host enzyme". Dissociation of NAD^+ from the same series of enzymes also exhibited biphasic kinetics with a transition to faster rates (a larger entropy of activation more than compensates for a larger enthalpy of activation) at temperatures of 41, 38, 36, and 29 °C, respectively. This order is also consistent with changes in helix 18 but again requiring influence of other properties of the "host enzyme". Global unfolding of all fully reconstituted holoenzymes occurred around 63 °C, confirming that the kinetic transition temperatures did not arise from a major disruption of the protein structure.

AdoHcy[1] is a product and also a potent feedback inhibitor of numerous methyltransferases which use *S*-adenosyl-L-methionine (AdoMet) as methyl donor (*1, 2*). SAHH (EC 3.3.1.1), catalyzing the reversible conversion of AdoHcy to adenosine (Ado) and homocysteine (Hcy), plays a key role in maintaining the normal cellular level of AdoHcy. Inhibition of SAHH results in a cellular accumulation of AdoHcy, which inhibits AdoMet-dependent methyltransferases and causes a number of physiological and pharmacological effects (*1, 2*). Parasites such as *Leishmania donovani*, *Plasmodium falciparum*, and *Trypanosoma cruzi* have their own SAHHs (*3–5*), and antiparasitic effects have been observed *in vitro* and *in vivo* by using known inhibitors of SAHH (*6–8*). Thus SAHH is a potential target for antiparasitic drugs.

SAHH is a homotetrameric protein containing four tightly bound molecules of NAD^+ as cofactors. Scheme 1 shows the catalytic cycle of the enzyme and the role of the cofactor in activating the elimination and addition reactions within it (*9*); in Scheme 1, the subscripts "O" and "C" refer to the "open" and "closed" forms of the enzyme (*1, 9*). The X-ray

[†] This research was supported by Grant GM-29332 from the National Institute of General Medical Sciences and by the K-INBRE Bioinformatics Core, NIH Grant P20 RR016475.

* To whom correspondence should be addressed at the Department of Pharmaceutical Chemistry, The University of Kansas. Tel: 785-864-4080. Fax: 785-864-5736. E-mail: rschowen@ku.edu.

[‡] Department of Pharmaceutical Chemistry.

[§] Department of Molecular Biosciences.

[||] Bioinformatics Core Facility.

[⊥] Department of Chemistry.

[1] Abbreviations: 2 × YT medium, 2 × yeast extract tryptone medium; Ado, adenosine; AdoHcy, *S*-adenosyl-L-homocysteine; CD, circular dichroism; DSC, differential scanning calorimetry; EDTA, ethylenediaminetetraacetic acid; FPLC, fast protein liquid chromatography; Hcy, L-homocysteine; HPLC, high-performance liquid chromatography; Hs-18Pf-SAHH, Hs-SAHH mutant (E411D/K412N/A414C/Y416F) with helix 18 replaced by helix 18 from Pf-SAHH; Hs-18Tc-SAHH, Hs-SAHH mutant (E411A/K412R/Q415D) with helix 18 replaced by helix 18 from Tc-SAHH; Hs-SAHH, SAHH from *Homo sapiens* (human placenta); Ld-SAHH, SAHH from *Leishmania donovani*, *L. donovani*, *Leishmania donovani*; NAD^+, β-nicotinamide adenine dinucleotide; NADH, β-nicotinamide adenine dinucleotide, reduced form; PCR, polymerase chain reaction; *P. falciparum*, *Plasmodium falciparum*; Pf-SAHH, SAHH from *Plasmodium falciparum*; SAHH, *S*-adenosyl-L-homocysteine hydrolase (EC 3.1.1.1); S-NAD^+, β-thionicotinamide adenine dinucleotide; S-NADH, β-thionicotinamide adenine dinucleotide, reduced form; Tc-18Hs-SAHH, Tc-SAHH mutant (A416E/R417K/D420Q/I422L) with helix 18 replaced by helix 18 from Hs-SAHH; Tc-SAHH, SAHH from *Trypanosoma cruzi*; *T. cruzi*, *Trypanosoma cruzi*.

10.1021/bi800175g CCC: $40.75
Published on Web 04/08/2008

Scheme 1: Schematic Catalytic Cycle for SAHHs

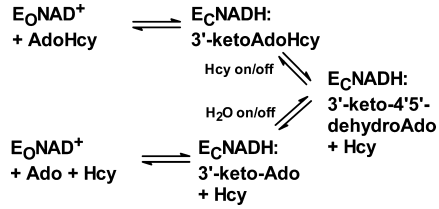

crystallographic structures of Hs-SAHH (*9*), Pf-SAHH (*10*), and Tc-SAHH (*11*) indicate a unique binding site for the cofactor, composed in part by elements of a penetrating C-terminal extension from an adjacent subunit. The C-terminal extension is crucial in maintaining the activity and quaternary structure of SAHH (*12, 13*).

Although direct interactions between the cofactor and polypeptide that would normally be considered key interactions, including the interactions with the C-terminal extension of the adjacent monomer, are generally conserved in the human and parasitic enzymes, significant differences in the kinetics and thermodynamics of NAD^+ binding among the human and parasitic enzymes have been observed (*3, 5, 14*). Our previous work indicated that there may be some local elements near the cofactor binding site which play an important role in NAD^+ binding (*14*). Helix 18 (Figure 1), for example, terminates in a loop containing residues that interact with NAD^+. In this paper, we present information that supports the hypothesis that helix 18 is an important element for human-parasitic distinctions in cofactor binding to SAHHs.

MATERIALS AND METHODS

Site-Directed Mutagenesis. All mutants were created by site-directed mutagenesis PCR. Each amplification reaction contained the following in a volume of 50 μL: 25 pmol of each primer, 20 nmol of each deoxynucleoside triphosphate, 20 ng of template DNA, 6 μL of 10× Pfu DNA polymerase buffer, and 3 units of Pfu DNA polymerase (Stratagene). Sequences of primers used for site-directed mutagenesis were as follows: 5′-GCTAACTGATAACCAATGCCAGTACCTGGG-3′ and 5′-CCCAGGTACTGGCATTGGTTATCAGTTAGC-3′ for Hs-SAHH; 5′-GACGAAGCTCACCGAGAAGCAGGCGCAGTACCTCGGCTGCCCCGT-3′ and 5′-ACGGGGCAGCCGAGGTACTGCGCCTGCTTCTCGGTGAGCTTCGTC-3′ for Tc-SAHH. After 4 min of a heat-start step at 92 °C, 25 cycles of the following program were initiated: 20 s at 92 °C, 30 s at 55 °C, and 20 min at 68 °C. PCR products were purified with a PCR purification kit (Qiagen). After treatment with *Dpn*I (Biolab), the PCR products were transformed into BL21(DE3) *Escherichia coli* (Stratagene). The sequences of mutant genes were confirmed by DNA sequencing.

Expression and Purification of Hs-SAHH, Tc-SAHH, and Their Mutants. The expression of Hs-SAHH, Tc-SAHH, and their mutants was basically the same as previously described (*3, 5*). Briefly, the genes encoding the enzymes were inserted in the vector pPROK-1 (Clonetech), and the recombinant plasmids were transferred into *E. coli* strain JM109. The transformed *E. coli* cells grew in 1 L of 2 × YT medium containing ampicillin (100 mg/L) at 37 °C. At OD_{600} = 0.4−0.8, 1 mM isopropyl 1-thio-β-D-galactopyranoside was added to induce protein expression at 37 °C for 8 h for Hs-SAHH and its mutants and at 25 °C for 12 h for Tc-SAHH and its mutant.

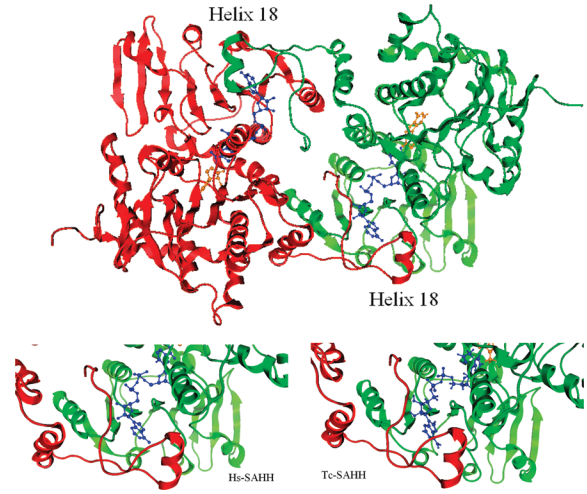

FIGURE 1: Above: Dimeric association of two monomeric subunits (red and green) within the tetrameric structure of Hs-SAHH (PDB code 1A7A) showing the C-terminal extensions containing helix 18 which penetrate into the adjacent subunit. Helix 18 is relatively near the cofactor (blue) and relatively distant from the substrate (yellow substrate-analogue structure). Below: Detail of the helix-18 region in Hs-SAHH and Tc-SAHH (PDB code 1XBE) showing the C-terminal loop that proceeds from helix 18 and interacts with the cofactor.

The procedures for purification of these enzymes were the same as previously described (*3, 5*) except that 50 μM NAD^+ was added to the buffer for the purification of Tc-SAHH and its mutant. The harvested *E. coli* cells containing the enzyme were stored at –80 °C. Cell-free extraction was carried out as previously described (*3, 5*). The enzyme was purified from cell-free extract by means of four columns in an FPLC system (Amersham Biosciences). The buffer for all purification processes was 50 mM Tris-HCl, pH 7.4, containing 1 mM EDTA. A typical procedure follows. The cell-free extract was loaded onto the first column, a Q-Sepharose fast-flow column (26/10), and the enzyme was eluted with 50−150 mM NaCl in buffer. Then the enzyme sample was loaded onto the second column, a HiLoad phenyl-Sepharose column (26/10). Neither Hs-SAHH nor Tc-SAHH binds to this column. The eluted enzyme was further purified by a third column, a HiLoad Superdex 200 (16/60) column. The fully purified enzyme was finally obtained from the fourth column, a MonoQ (10/10) column, by elution with 50−300 mM NaCl in buffer. The purities of all fully purified enzymes were estimated at 99% by observation of a single band with molecular weight corresponding to that of the monomeric enzyme on SDS−PAGE (staining with Coomassie blue, loading up to 10 μg of protein per lane, with detection sensitivity estimated at 0.1 μg of protein).

Enzyme Activity Assay and Determination of Kinetic Properties. SAHH activities were assayed in the synthetic direction by measuring the rate of formation of AdoHcy from Ado and Hcy by an HPLC method previously described (*15, 16*). The enzyme activity in the hydrolytic direction was determined by coupling the AdoHcy hydrolysis reaction to Ado deamination catalyzed by Ado deaminase as previously described (*16*). The enzyme kinetic parameters (K_m and k_{cat}) were obtained by least-squares fitting of the activity data at

various substrate concentrations to the Michaelis–Menten equation with Origin version 7.5 software (Microcal Software, Northampton, MA).

Determination of Apoenzyme Concentration by NAD$^+$ Titration. Apoenzyme was prepared as previously described (*17*). All enzyme and apoenzyme concentrations in this paper are given as molar concentrations of the monomeric subunit. Because NAD^+ binds to all four SAHHs very tightly at 22 °C (K_d below 50 nM at 22 °C for all enzymes), the concentration of apoenzyme can be determined from enzyme-activity measurements with NAD^+ titration as described previously (*14*).

Determination of the Rate Constants (k_{off}) for Dissociation of NAD$^+$ from Hs-18Pf-SAHH and Tc-18Hs-SAHH. The measurements were carried out as described previously (*14*). Briefly, NAD^+ was allowed to dissociate from fully reconstituted enzyme in the presence of excess NADH which irreversibly traps each vacated binding site. The decrease in enzyme activity occurred in a first-order fashion with a rate constant $k_{obs} = k_{off} + k_{ina}$, where k_{ina} is the first-order rate constant for thermal inactivation, determined in control experiments. The dissociation rate constants k_{off} were calculated as $k_{off} = k_{obs} - k_{ina}$.

Determination of Rate Constants for Association of NAD$^+$ with Apoenzymes (Apparent First-Order Rate Constant k_{app} and Apparent Second-Order Rate Constant k_0). This process was executed as described previously (*14*). Typically, a 50 μL solution (50 mM phosphate buffer, pH 7.4, 1 mM EDTA) containing 2 μM apoenzyme was added to a preincubated 50 μL aliquot of 10 μM NAD^+ solution. Samples were taken for activity assay at measured times during incubation at the desired temperature. The measured activities A were either converted to the amount of enzyme−NAD^+ complex or used directly in eq 1.

$$A = A_f + (A_0 - A_f)[\exp(-k_{app}t)] \quad (1)$$

Here, A is the activity measured at time t, A_0 is the activity at the apparent time zero (reflecting reaction during the dead time of the experiment), A_f is the activity at the end of the experiment, and k_{app} is a first-order rate constant for association that generally will be a function of [NAD^+]. At [NAD^+] = 5 μM, A_0 is quite small and k_{app} is approximately proportional to [NAD^+]; an apparent second-order rate constant for the association reaction k_0 was therefore calculated from data at this concentration as $k_0 = k_{app}/[NAD^+]$.

Differential Scanning Calorimetry (DSC). Measurements were made with three different kinds of solutions: (1) apoenzyme, (2) holoenzyme (purified from *E. coli* cells, fully occupied by cofactor, approximately 95% NAD^+ and 5% NADH), and (3) holoenzyme in the presence of 1–20 mM NAD^+. All samples (2 mg/mL of enzyme) were degassed under mild vacuum for 15 min before the measurement of thermograms with a Microcal DSC instrument (Northampton, MA). An aliquot of a solution (0.9 mL) of buffer containing 50 mM phosphate and 1 mM EDTA, pH 7.4, with or without 1–20 mM NAD^+, was placed in the reference cell, and an enzyme sample in the same buffer was placed in the sample cell. Thermograms from 25 to 80 °C were collected at a scan rate of 60 °C/h. Control scans obtained with buffer in both the reference and sample cells were subtracted from the thermograms.

Table 1: Sequences and Total Helix Propensity Values for Helix 18 of Hs-SAHH, Tc-SAHH, Ld-SAHH, and Pf-SAHH[a]

SAHH	sequence$_{(\text{propensity value})}$	total helix propensity
Hs (411–417)	$E_{(1.37)}K_{(1.14)}Q_{(1.34)}A_{(1.46)}Q_{(1.34)}Y_{(0.95)}L_{(1.36)}$	8.96
Tc (416–422)	$A_{(1.46)}R_{(1.24)}Q_{(1.34)}A_{(1.46)}D_{(0.83)}Y_{(0.95)}I_{(1.07)}$	8.35
Ld (416–422)	$P_{(0.40)}K_{(1.14)}Q_{(1.34)}A_{(1.46)}E_{(1.37)}Y_{(0.95)}I_{(1.07)}$	7.73
Pf (459–465)	$D_{(0.83)}N_{(0.72)}Q_{(1.34)}C_{(0.75)}Q_{(1.34)}F_{(0.97)}L_{(1.36)}$	7.31

[a] Individual sequence ranges for the helix are shown beneath the species identifier at the left, and the residue helix propensities are shown as subscripts.

Circular Dichroism (CD) Spectroscopy. CD spectra were measured with a Jasco J-720 spectropolarimeter equipped with a Peltier temperature controller. Enzyme samples (apo form or holo form, 0.1 mg/mL in 50 mM phosphate buffer, pH 7.4, and 1 mM EDTA) were placed in 0.1 cm path length cells. A resolution of 0.2 nm and a scanning speed of 20 nm/min with a 2 s response time were employed. Results presented are from an average of three consecutive spectra. For the thermal studies, the signal at 222 nm was measured at 0.1 °C intervals with use of a 60 °C/h temperature ramp rate.

Temperature-Dependent Fluorescence Spectroscopy of Tc-SAHH and Tc-18Hs-SAHH in the Presence of 8-Anilino-1-naphthalenesulfonic Acid. Fluorescence emission spectra of holo-Tc-SAHH and its mutant holo-Tc-18Hs-SAHH (5.15 μM) in a solution containing a molar ratio of 12:1 ([dye]:[monomer]) of 8-anilino-1-naphthalenesulfonic acid over protein were obtained using a QuantaMaster spectrofluorometer (PTI, Monmouth Junction, NJ). The excitation wavelength was 372 nm, and the emission was monitored at 480 nm over a range of temperature from 15 to 77.5 °C at 2.5 °C intervals.

RESULTS

The Stability of Helix 18 in SAHHs, Estimated from Helix Propensities, Is Greater for Hs-SAHH Than for Tc-SAHH, Ld-SAHH, and Pf-SAHH. The helix propensity of each helix 18 is the sum of the helix propensities of all residues in the helix (Figure 1, Table 1). A good measure of the helix propensity of a residue is the relative frequency with which the residue is present in helices, as calculated by Kallberg et al. from a nonredundant set of protein sequences with known three-dimensional structures (1324 proteins, total of 269058 amino acid residues) by PHD (profile network from HeiDelberg) (*14, 18*). Helix-propensity values are typically used to predict secondary structure. Here, however, we presume that a helix with a higher total helix-propensity value may be more stable and therefore show less mobility and flexibility. As shown in Table 1, the helix propensities of helix 18 in Hs-SAHH and Pf-SAHH are the highest and the lowest, respectively.

Generation of SAHH Mutants with Altered Structures of Helix 18. With guidance from the total helix propensities in Table 1, three mutant enzymes were created and compared to Hs-SAHH and Tc-SAHH. The mutants are (1) a Hs-SAHH mutant with its original helix 18 replaced with the one from Tc-SAHH and denoted Hs-18Tc-SAHH, (2) a Tc-SAHH mutant with its original helix 18 replaced with the one from Hs-SAHH and denoted Tc-18Hs-SAHH, and (3) a Hs-SAHH mutant with its original helix 18 replaced with the one from

Table 2: Kinetic Parameters[a] for Hs-SAHH, Hs-18Tc-SAHH, Tc-SAHH, Tc-18Hs-SAHH, and Hs-18Pf-SAHH Measured in 50 mM Phosphate Buffer, pH 7.4, and 1 mM EDTA at 37 °C

kinetic parameter	Hs-SAHH	Hs-18Tc-SAHH	Hs-18Pf-SAHH	Tc-18Hs-SAHH	Tc-SAHH
			[Ado] Varied for Synthesis of AdoHcy		
k_{cat} (s^{-1})	12.5 ± 0.2	13.2 ± 0.4	11.8 ± 0.2	15.0 ± 0.5	15.5 ± 0.3
K_m (μM)	1.5 ± 0.1	1.4 ± 0.1	1.1 ± 0.1	2.0 ± 0.2	1.2 ± 0.1
			[Hcy] Varied for Synthesis of AdoHcy		
k_{cat} (s^{-1})	16.2 ± 0.9	16.9 ± 1.1	14.6 ± 1.2	15.6 ± 0.6	16.7 ± 1.1
K_m (μM)	160 ± 28	171 ± 24	188 ± 27	100 ± 12	219 ± 26
			[AdoHcy] Varied for Hydrolysis of AdoHcy		
k_{cat} (s^{-1})	3.2 ± 0.1	3.3 ± 0.1	3.2 ± 0.1	3.2 ± 0.2	3.7 ± 0.1
K_m (μM)	6.4 ± 0.4	6.2 ± 0.4	5.8 ± 0.4	14.3 ± 0.3	3.2 ± 0.3

[a] Standard deviations were obtained from least-squares fitting with Origin software, version 7.5. The fit was carried out with mean values from three experiments.

Pf-SAHH and denoted Hs-18Pf-SAHH. The set of helix-18 mutants thus includes the "trypanosomized" human enzyme, the "humanized" trypanosomal enzyme, and a "plasmodiumized" human enzyme. This last mutant, Hs-18Pf-SAHH, represents the human enzyme modified to have the helix 18 of lowest total helical propensity present in any of the parasitic enzymes.

The mutant enzymes as well as the two wild-type enzymes Hs-SAHH and Tc-SAHH were expressed, purified, and characterized under very similar conditions. In all cases, it was determined by CD that the secondary structure was not detectably changed and by size-exclusion chromatography that the tetrameric quaternary structure was intact. All enzymes were fully reconstituted with oxidized cofactor.

Catalytic Kinetic Constants of Helix-18 Mutant Enzymes Differ Little from Those of the Wild-Type Enzymes. Results of kinetic studies of Hs-SAHH, Tc-SAHH, and their helix-18 mutants are shown in Table 2. All enzymes exhibit nearly the same values for both the synthesis and hydrolysis of AdoHcy, minor exceptions being (1) the K_m for AdoHcy of Hs-SAHH is twice that of of Tc-SAHH; (2) K_m values for Hcy and AdoHcy of Tc-18Hs-SAHH are about half and four times, respectively, those of Tc-SAHH. The indication is thus that these mutations, relatively remote from the center of catalysis, have no major effects on catalysis.

The Kinetics of the Dissociation of NAD$^+$ from Hs-18Pf-SAHH and Tc-18Hs-SAHH Show the Same Biphasic Temperature Dependences Observed with Hs-SAHH and Tc-SAHH. Eyring plots of the first-order rate constants k_{off} for dissociation of the cofactor NAD$^+$ from Hs-18Pf-SAHH (31−45.5 °C) and from Tc-18Hs-SAHH (21−45.5 °C) are similar to the ones for the two wild-type enzymes (Figure 2): the dependences are nonlinear for both enzymes, consisting of a linear low-temperature regime and a linear high-temperature regime. Data for the two temperature regimes were independently fitted by the Eyring equations (eqs 2a and 2b) as before (*14*).

$$k_{off}/(kT/h) = \exp[(\Delta S^{\ddagger}_{l}/R) - (\Delta H^{\ddagger}_{l}/RT)] \quad (2a)$$

$$k_{off}/(kT/h) = \exp[(\Delta S^{\ddagger}_{h}/R) - (\Delta H^{\ddagger}_{h}/RT)] \quad (2b)$$

Here, the subscript l denotes the quasi-thermodynamic parameters of activation for the low-temperature regime and the subscript h denotes those for the high-temperature regime. The values of the quasi-thermodynamic parameters of activation are given in Table 3. The conversion temperature

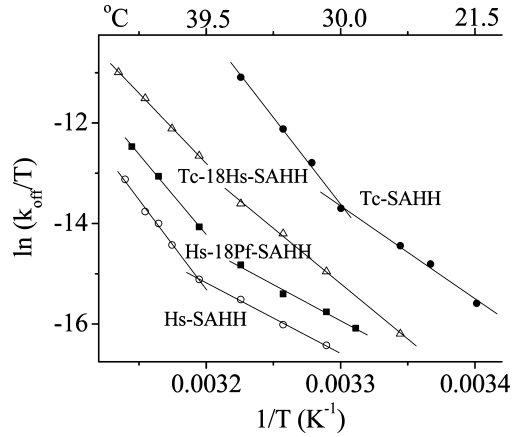

FIGURE 2: Temperature dependence of the rate constant k_{off} for dissociation of NAD$^+$ from Hs-SAHH, Hs-18Pf-SAHH, Tc-18Hs-SAHH, and Tc-SAHH. The lines are intersecting Eyring plots with the parameters given in Table 3.

T_0 for passage from the low-temperature regime to the high-temperature regime was calculated from eq 3 (*14*), and values are also given in Table 3.

$$T_0 = (\Delta H^{\ddagger}_{h} - \Delta H^{\ddagger}_{l})/(\Delta S^{\ddagger}_{h} - \Delta S^{\ddagger}_{l}) \quad (3)$$

Figure 2 shows that the mutants Hs-18Pf-SAHH and Tc-18Hs-SAHH produce behavior that is intermediate between those of the two wild-type enzymes from which they derive. Table 3 shows that, as with the wild-type enzymes, a low-enthalpy, small positive entropy dependence at low temperatures is replaced by a high-enthalpy, large positive entropy change at high temperatures (the data are not persuasively biphasic for Tc-18Hs-SAHH, but a break is visually detectable).

The Slow-Binding Kinetics of the Association of NAD$^+$ with Apo-Hs-18Pf-SAHH and Apo-Tc-18Hs-SAHH Show the Same Biphasic Temperature Dependences Observed with Hs-SAHH and Tc-SAHH. The wild-type enzymes were earlier found (*14*) to exhibit both a fast-binding phase (within the instrumental dead time) and a slow-binding phase for the association of the apoenzymes with NAD$^+$. The fast-binding phase was negligible at concentrations of NAD$^+$ of 5 μM and lower. Here the mutant enzymes were studied at 5 μM NAD$^+$. The first-order rate constants k_{app} for association of NAD$^+$ with Hs-18Pf-SAHH and Tc-18Hs-SAHH were measured at 5 μM NAD$^+$ and used to calculate the second-order rate constants k_0, as k_{app}/[NAD$^+$] (*14*). Figure 3 presents the Eyring plots of the slow-binding rate constants k_0

Table 3: Quasi-Thermodynamic Parameters of Activation for Low-Temperature and High-Temperature Regimes and Conversion Temperatures[a] T_0 between Regimes for NAD^+ Dissociation from Tc-SAHH (21−37 °C), Tc-18Hs-SAHH (26−46.5 °C), Hs-18Pf-SAHH (29−45.5 °C), and Hs-SAHH (31−45.5 °C) at pH 7.4

enzyme	$\Delta S^{\ddagger}_l$ [J/(mol·K)]	$\Delta H^{\ddagger}_l$ (kJ/mol)	$\Delta S^{\ddagger}_h$ [J/(mol·K)]	$\Delta H^{\ddagger}_h$ (kJ/mol)	T_0, K
Tc-SAHH	170 ± 15	154 ± 8	610 ± 30	287 ± 8	302 ± 34 (29 °C)
Tc-18Hs-SAHH	274 ± 1	181 ± 1	438 ± 9	232 ± 4	309 ± 11 (36 °C)
Hs-18Pf-SAHH	64 ± 7	119 ± 8	533 ± 18	265 ± 8	311 ± 19 (38 °C)
Hs-SAHH	50 ± 2	116 ± 4	600 ± 25	297 ± 9	314 ± 21 (41 °C)

[a] Temperature of intersection of the high-temperature and low-temperature limbs of the temperature dependence and thus the apparent temperature of conversion between the two regimes.

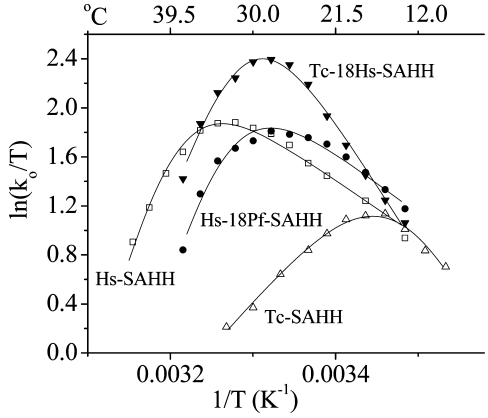

FIGURE 3: Temperature dependence of the rate constant for the slow-binding phase of the association of NAD^+ with the apo forms of Hs-SAHH, Hs-18Pf-SAHH, Tc-18Hs-SAHH, and Tc-SAHH. The lines are plots of eq 4 with the parameters shown in Table 4.

measured over a range of temperatures. A few representative points (not shown) were measured for Hs-18Tc-SAHH but were found to lie directly on the line for Hs-SAHH. We conclude that at least this property and perhaps others of Hs-SAHH are not altered by the 18Tc mutation. We therefore turned to Hs-18Pf-SAHH for further studies. The association kinetics and their temperature dependences for both Hs-18Pf-SAHH and Tc-18Hs-SAHH are distinctly different from the two wild-type enzymes and from each other (Figure 3).

A model developed previously (*14*) from similar data for the wild-type enzymes ascribes the decrease in association rate at higher temperatures to a (perhaps local) reversible unfolding phenomenon. The temperature dependence of the apparent association constant k_0 is then described by eq 4, where we take the standard-state concentration of NAD^+, $[NAD^+]_{ss} = 1$ M:

$$\ln(k_0/T) = (\Delta S^{\ddagger}_{on}/R) - (\Delta H^{\ddagger}_{on}/RT) - \ln\{1 + \exp[(\Delta S^{\circ}_{un}/R) - (\Delta H^{\circ}_{un}/RT)]\} - \ln[NAD^+]_{ss} + \ln(k/h) \quad (4)$$

Here the subscript "on" denotes the quasi-thermodynamic parameters of activation for cofactor binding, and the subscript "un" denotes the thermodynamic parameters of the reversible unfolding process (thus $k_0 = k_{on}/[1 + K_{un}]$). The values of the enthalpies and entropies are given in Table 4. The table also gives the ratio $\Delta H^{\circ}_{un}/\Delta S^{\circ}_{un}$ as a rough measure of the "melting temperature" for the presumed local structural transition.

Thermal Structural Perturbation of Wild-Type Enzymes and Helix-18 Mutants Analyzed by DSC and CD. Figure 4 presents thermograms obtained from DSC studies of wild-type and mutant enzymes as apoenzymes, holoenzymes, and holoenzyme in the presence of 20 mM NAD^+. All of the proteins showed an irreversible thermal unfolding process. A sharp reduction in heat capacity indicated that aggregation ensued rapidly after unfolding. Therefore, thermodynamic analysis by fitting data to models for reversible phase-transition processes is not possible. Thus, we hereafter use the term "stability" in this connection in a casual, nonthermodynamic sense simply to reflect changes in response of the protein to temperature variation, as detected by DSC and the spectroscopic techniques described below. Light-scattering measurements (data not shown) confirmed that aggregation followed unfolding.

Table 5 shows the apparent melting temperatures, which were taken to be the temperatures at which a maximum heat capacity was observed (Figure 4). In addition, data for CD observations are included in Table 5, and these agree with the DSC results in all cases.

Table 5 shows that apo-Hs-SAHH is somewhat less thermally stable than apo-Tc-SAHH but that this difference is erased in the holoenzymes, and excess cofactor raises the melting temperatures of both enzymes further, either by assuring full cofactor occupancy or by nonspecific binding and stabilization. The observation that holo-Tc-SAHH melts at the same temperature as apo-Tc-SAHH is the result of an artifact: the DSC thermogram (Figure 4) shows that the cofactor dissociates at about 42 °C, so that the melting event at 53 °C reflects, in fact, the melting of the apoenzyme (see also Figure 5).

The mutant Tc-18Hs-SAHH does not produce evidence in the data of Figure 5 for such an anomaly, but the single peak in the thermogram of Figure 4 is very broad, consistent with dissociation of the cofactor simultaneously with the larger structural changes. Consistent with this explanation, addition of excess cofactor produces a sharp peak in the thermogram, presumably by maintaining a high population of bound cofactor during global unfolding. The mutant Hs-18Pf-SAHH melts at slightly lower temperatures than the parent Hs-SAHH but is otherwise unremarkable with respect to more extensive unfolding.

All holoenzymes exhibit, in the presence of excess NAD^+, very similar apparent melting temperatures around 62−65 °C as expected for their high sequence similarity and consistent with the composition of helix 18 having little or no influence on global unfolding.

The apoenzymes apo-Hs-SAHH and apo-Hs-18Pf-SAHH show similar melting temperatures of 44 and 41 °C, respectively, while the apo-Tc-SAHH and apo-Tc-18Hs-SAHH both melt at 53 °C, consistent with a somewhat greater global stability for Tc-SAHH than for Hs-SAHH, with the mutated helix 18 producing no change in the thermal behavior of the wild-type enzyme. The holoenzymes uniformly melt about 10−11 °C higher than do the apoenzymes,

Table 4: Thermodynamic and Quasi-Thermodynamic Parameters[a] for NAD^+ Association with Tc-SAHH, Tc-18Hs-SAHH, Hs-18Pf-SAHH, and Hs-SAHH at Temperatures in the Interval 11−45 °C, pH 7.4

enzyme	$\Delta S^{\ddagger}_{on}$ [J/(K•mol)]	$\Delta H^{\ddagger}_{on}$ (kJ/mol)	ΔS°_{un} [J/(K•mol)]	ΔH°_{un} (kJ/mol)	$\Delta H^{\circ}_{un}/\Delta S^{\circ}_{un}$ (K)
Tc-SAHH	225 ± 13	118 ± 4	631 ± 8	182 ± 2	288 ± 5 (15 °C)
Tc-18Hs-SAHH	119 ± 19	89 ± 6	815 ± 5	247 ± 1	303 ± 2 (30 °C)
Hs-18Pf-SAHH	−42 ± 16	42 ± 5	765 ± 7	234 ± 2	306 ± 4 (33 °C)
Hs-SAHH	−56 ± 9	38 ± 3	788 ± 5	243 ± 2	308 ± 3 (35 °C)

[a] Parameters were obtained by least-squares fitting to eq 4 (Origin version 7.5). The subscript "on" identfies the quasi-thermodynamic parameters of activation for the binding rate constant of the slow-binding phase of cofactor binding. The subscript "un" identfies the equilibrium thermodynamic parameters for local unfolding in or near the cofactor binding site.

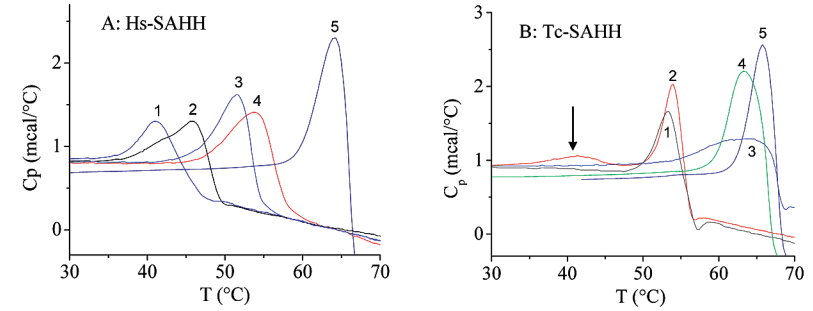

A:
1. apo-Hs-18Pf-SAHH
2. apo-Hs-SAHH
3. holo-Hs-18Pf-SAHH
4. holo-Hs-SAHH
5. holo-Hs-SAHH, 20 mM NAD^+.

B:
1. apo-Tc-SAHH
2. holo-Tc-SAHH
3. holo-Tc-18Hs-SAHH
4. holo-Tc-SAHH, 20 mM NAD^+
5. holo-Tc-18Hs-SAHH 20 mM NAD^+.

FIGURE 4: DSC thermograms from 30 to 70 °C of the apo and holo forms of Hs-SAHH, Hs-18Pf-SAHH, Tc-18Hs-SAHH, and Tc-SAHH.

Table 5: Apparent Melting Temperatures (°C)[a] from Differential Scanning Calorimetry (DSC, Figure 4) for the Apoenzyme and Holoenzyme Forms (the Latter Also in the Presence of 20 mM NAD^+) of Tc-SAHH, Tc-18Hs-SAHH, Hs-18Pf-SAHH, and Hs-SAHH and Similar Data for Apoenzymes and Holoenzymes from Circular Dichroism (CD), Determined from the Midpoints of Thermal Unfolding Curves

	DSC			CD	
enzyme	apo	holo	holo + 20 mM NAD^+	apo	holo
Tc-SAHH	53.0 ± 0.2	53.2 ± 0.2	62.1 ± 0.4	54.0 ± 0.2	54.0 ± 0.2
Tc-18Hs-SAHH	53.0 ± 0.1	63.4 ± 0.2	65.2 ± 0.3	54.1 ± 0.2	62.0 ± 0.3
Hs-18Pf-SAHH	41.3 ± 0.2	51.4 ± 0.1	62.8 ± 0.5	41.2 ± 0.3	52.4 ± 0.5
Hs-SAHH	44.2 ± 0.1	55.2 ± 0.3	63.6 ± 0.4	44.4 ± 0.2	55.4 ± 0.3

[a] Errors were obtained from the range of two independent measurements.

consistent with thermal stabilization by the cofactor, except for the anomalous holo-Tc-SAHH (see above).

DISCUSSION

The Total Helix Propensities of Helix 18 and Structures for Human and Parasitic SAHHs Suggest Lower Stability and Perhaps Larger Mobility for the Parasitic Helices. Helix 18 in the structure of SAHHs is relatively distant from the substrate-binding region and the surrounding catalytic residues (*19*) of the active site but relatively close to the cofactor binding site (Figure 1). Helix 18 therefore seemed an attractive possibility for a significant contribution to the distinct kinetics and thermodynamics of cofactor association and dissociation observed for Hs-SAHH and Tc-SAHH, while at the same time conserving the catalytic kinetic properties of the two enzymes. We explored this hypothesis initially by use of helix propensities, supported by X-ray structures.

Table 1 shows the sequences in the helix-18 regions of Hs-SAHH, Tc-SAHH, Ld-SAHH, and Pf-SAHH, together with the total helix propensity for helix 18 in each of the enzymes. As predictors that a peptide segment will assume a helical conformation in a statistically averaged protein environment (*18*), helix propensities are limited by the omission of effects from nearby residues and their side chains in the primary sequence and the effect of environmental factors not accounted for in the statistical average. X-ray crystallographic structural data, now available (*9, 10*) for Hs-SAHH, Pf-SAHH, and Tc-SAHH, however, indicate some mitigating factors. Helix 18 in all of these SAHHs is located on the enzyme surface and makes few interactions with other parts of the protein (Figure 6).

All of the interactions identified in Figure 6 suggest a greater stability for Hs-SAHH, and secondarily for Tc-SAHH, than for the other enzymes. Furthermore, the negatively charged E411, near the N-terminus of helix 18 in Hs-SAHH, should interact favorably with the helix dipole (*20, 21*) but is replaced by electrically neutral residues in two of the three parasitic enzymes (Table 1). The electrically neutral Q415 toward the C-terminus of the helix

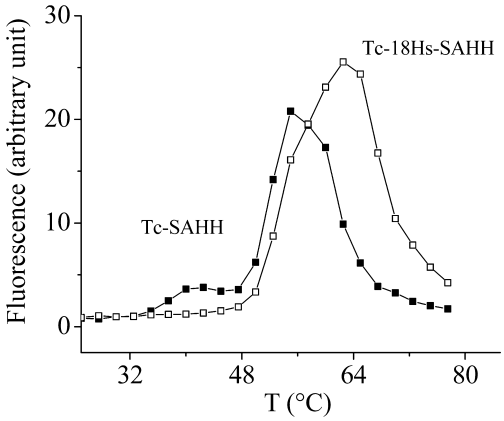

FIGURE 5: Thermally induced fluorescence changes for Tc-SAHH and Tc-18Hs-SAHH in the presence of the dye 8-anilino-1-naphthalenesulfonate, which fluoresces when bound in a nonpolar environment. At 42 °C, the cofactor dissociates from Tc-SAHH, and the dye occupies the cofactor site. No such dissociation is seen with Tc-18Hs-SAHH. The large maxima result from global unfolding of apo-Tc-SAHH and of holo-Tc-18Hs-SAHH.

in Hs-SAHH is replaced by destabilizing (*20, 22*) negatively charged residues in two of the three parasitic enzymes.

Therefore, the helix-propensity prediction (Table 1) of a stability order for helix 18 of Hs-SAHH > Tc-SAHH > Ld-SAHH > Pf-SAHH appeared sufficiently supported by structural data to encourage further investigation of the effects of helix-18 sequences on cofactor binding and other properties of the human and parasitic enzymes. In addition to serving as indicators of helix stability, the helix propensities seemed to be possible indicators of the subtler property of helix mobility or flexibility. If it is assumed that a more stable or immobile helix 18 would provide a more stable cofactor binding site, then the results are consistent with the observation that the human enzyme binds NAD^+ more tightly than the parasitic enzymes (*3, 5, 14*).

Catalytic Properties of Wild-Type and Mutant Enzymes. Investigations of the role of helix 18 in the distinct properties of human and parasitic enzymes were pursued through construction of three mutants for comparison with wild-type enzymes: (1) Hs-18Tc-SAHH, the human enzyme bearing the helix 18 of Tc-SAHH in place of its own, (2) Tc-18Hs-SAHH, the trypanosomal enzyme containing the helix 18 of Hs-SAHH, and (3) Hs-18Pf-SAHH, the human enzyme with the helix 18 of Pf-SAHH. As will be described below, the properties of Hs-18Tc-SAHH were found at an early point in this work to be essentially indistinguishable from those of Hs-SAHH. Therefore, Hs-18Pf-SAHH was prepared with the sequence of helix 18 as that of lowest helix propensity; indeed, the properties of this mutant were different from those of Hs-SAHH, and further studies made use of this mutant. As expected, mutations in helix 18, quite distant from the catalytic site, produced no major changes in the catalytic properties of the wild-type enzymes, which are very similar to each other in this regard (Table 2).

Helix 18 Is Stabilized by the Binding of NAD^+, and a Thermally Induced Structural Change in or near Helix 18 Accelerates the Dissociation of NAD^+. The dissociation of NAD^+ from Hs-SAHH and Tc-SAHH was earlier found (*14*) to occur in a simple first-order fashion. For both enzymes, the rate constants increased with temperature biphasically,

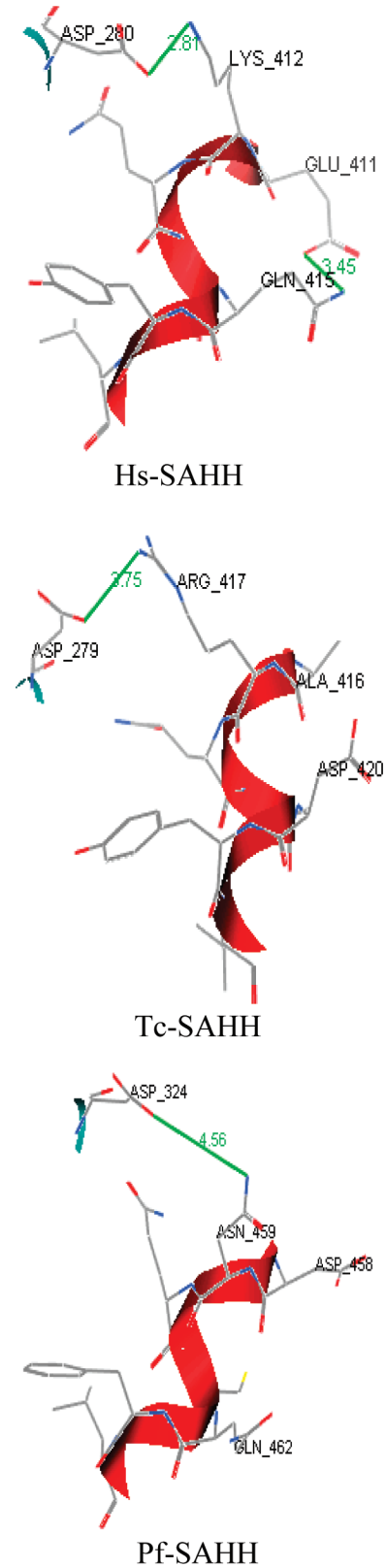

FIGURE 6: Hydrogen bonds formed between residues of helix 18 and nearby residues of the enzyme and among the residues within helix 18 for Hs-SAHH (external, K214−D280; internal, E411−N415), Tc-SAHH (external, R417−D279), and Pf-SAHH.

a transition occurring at 29 °C for Tc-SAHH and at 41 °C for Hs-SAHH. The transition altered a linear Eyring dependence with low enthalpy of activation and small positive entropy of activation (low temperatures) to a linear Eyring dependence with high enthalpy of activation and large

positive entropy of activation (high temperatures). The sharpness of the transition from a low-temperature to high-temperature regime suggests a structural transition as the origin of this relatively abrupt change. As elaborated below, changes in helix 18 seem to be a likely source of this behavior.

If the conversion between the two temperature regions is caused by a thermal perturbation of helix 18, then the activation parameters of Table 3 appear consistent with a view that the altered structure at higher temperatures binds the cofactor more tightly but generates substantially more entropy upon its release. A second point is that the apparent unfolding in the presence of the cofactor results in an accelerated dissociation of the cofactor. This involves a large positive entropy of activation that more than compensates for an increased enthalpy of activation. This finding would also be consistent with a greater mobility of the enzyme following the unfolding of helix 18 and dissociation of the cofactor.

Helix 18 (and/or Its Neighborhood) Is the Site of Local Structural Perturbation That Attenuates the Association of NAD^+ with Apo-SAHHs at Higher Temperatures. As described above, NAD^+ associates with Hs-SAHH and Tc-SAHH in a relatively complex manner that, in contrast to the catalytic properties, is quantitatively different for the two enzymes. Binding occurs in two phases, a fast-binding phase that occurs within the dead time of the measurement method and a slow-binding phase that occurs over some minutes and exhibits saturation with respect to the cofactor (*14*), with the results in Figure 3 and Table 4 referring to the slow-binding phase.

A striking difference in the wild-type enzymes is the local-unfolding temperature of about 35 °C for Hs-SAHH and about 15 °C for Tc-SAHH, as noted earlier (*14*). It was also earlier realized (*14*) that the structural alteration cannot correspond to global unfolding of the enzyme since that occurs in the range of 62–65 °C (Table 5).

The data for the two mutants, Hs-18Pf-SAHH and Tc-18Hs-SAHH, lend strong support to the hypothesis that the site of this local alteration is, in fact, helix 18. Introduction of the plasmodial helix 18 into the human enzyme shifts the perturbation temperature from 35 to 33 °C (although this shift is within the considerable error of the curve fit to the model, the phenomenological shift in the rate-constant maxima is clearly visible in Figure 3). More dramatically, introduction of the human helix 18 into the trypanosomal enzyme shifts this transition temperature in the opposite direction, from 15 to 30 °C, clearly beyond the errors of curve fitting and also readily visible in the temperature-dependent kinetic data of Figure 3. These results are consistent with the concept that helix 18 of Hs-SAHH is, as indicated by helix propensities and structural information, a more stable and perhaps rigid entity than is helix 18 of Tc-SAHH and Pf-SAHH.

Furthermore, the data suggest that the general context of helix 18 is more dynamic in Tc-SAHH than in Hs-SAHH. Thus, introduction of the more rigid human helix 18 into the presumably flexible environment of Tc-SAHH results in a large rise in the transition temperature, while introduction of the presumably most flexible plasmodial helix 18 into the rigid Hs-SAHH environment results in only a small downward shift of the transition temperature. The same idea can also explain the observation that the introduction of the trypanosomal helix 18 into the rigid Hs-SAHH matrix produces little or no effect.

Scheme 2: Temperature Effects on the Cofactor On-Rates and Off-Rates

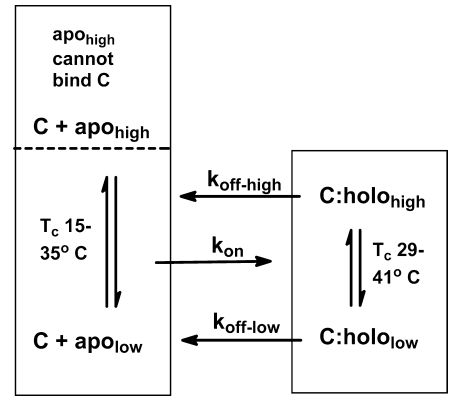

It should be noted that the approximate order of the transition temperatures of helix 18 in the apoenzymes, as here estimated from the cofactor association kinetics (Table 4), namely, Hs-SAHH (35 °C) > Hs-18Pf-SAHH (33 °C) > Tc-18Hs-SAHH (30 °C) > Tc-SAHH (15 °C), is the same as the order of the estimated conversion temperatures from the low-temperature to the high-temperature regime of the cofactor-dissociation kinetics (Table 3) discussed above, namely, Hs-SAHH (41 °C) > Hs-18Pf-SAHH (38 °C) > Tc-18Hs-SAHH (36 °C) > Tc-SAHH (29 °C). Admittedly, in some cases such comparisons fall well within the computed errors, but visual analysis of the figures lends support to their validity.

Most simply, the conversion temperatures for dissociation of cofactor are larger (29−41 °C) than the transition temperatures for its association (15−35 °C). This result would indicate that the helix has significantly greater thermal stability in the presence of the cofactor. Scheme 2 summarizes the situation. At the left, the apoenzyme consists of an equilibrium mixture of two forms: a high-temperature form incapable of binding the cofactor C and a low-temperature form capable of binding C, so that the on-reaction (rate constant k_{on}) proceeds from the fraction of apoenzyme in the low-temperature form. The conversion temperature between the two forms is 15–35 °C, and we suspect the conversion is a local structural change in or near helix 18. The holoenzyme at right likewise consists of an equilibrium mixture of low-temperature and high-temperature forms. Each releases the cofactor C but the high-temperature form does so more rapidly, with a steeper temperature dependence. The conversion temperatures here are larger, around 29–41 °C. Again, we suppose the conversion to be caused by local structural changes in or near helix 18. Conceivably the structural changes involved in the on-reaction and off-reaction are the same or similar, but the conversion temperatures tend to be higher for the off-reaction because the cofactor stabilizes helix 18 and its neighborhood.

Helix 18 Has Only a Minor Role in the Global Stability of SAHHs. The global unfolding temperatures given in Table 5 show that, for all forms of the wild-type and mutant enzymes, global unfolding occurs for apoenzymes in the range 41–65 °C and for holoenzymes in the range 51–65 °C. This is beyond the temperature range of 15–41 °C for

which structural alterations of helix 18 are proposed as the cause of the biphasic transitions observed in the kinetics of association and dissociation of the cofactor from SAHHs. This strongly suggests that the phenomenon involved in the cofactor association−dissociation kinetics is not due to the onset of global unfolding, but rather results from the proposed conformational changes in helix 18.

CONCLUSIONS

Previous studies (*14*) showed that the human enzyme Hs-SAHH and the parasitic enzyme Tc-SAHH have similar catalytic properties but differ distinctly in the on- and off-rates of the tightly bound NAD^+ cofactor. Structural information and calculations of helix propensities suggest that differences in the stability and possible mobility of helix 18, near the C-terminus and embedded into the cofactor binding site of the partner subunit, might account for these observations. Mutants were therefore constructed of the wild-type enzymes Hs-SAHH and Tc-SAHH in which the human helix 18 (predicted to be more stable and perhaps more rigid than the parasitic helices) has been replaced by a plasmodial helix 18 (predicted to be less stable), Hs-18Pf-SAHH, and in which the trypanosomal helix 18 (predicted to be of lower stability) has been replaced by the human helix 18 (Tc-18Hs-SAHH). These wild-type and mutant enzymes (1) exhibited essentially the same catalytic kinetic constants, (2) showed biphasic temperature dependences of the dissociation rate constants for NAD^+, with a thermal inflection reflecting structural changes in or near the cofactor binding sites, and the transition temperatures sytematically varying from 29 °C (Tc-SAHH) to 41 °C (Hs-SAHH), the two mutants falling between these limits, (3) showed biphasic temperature dependences of the association rate constants for NAD^+, with a thermal maximum reflecting local changes in or near the cofactor binding sites, and the transition temperatures sytematically varying from 15 °C (Tc-SAHH) to 35 °C (Hs-SAHH), the two mutants again falling between these limits, and (4) underwent more global unfolding at temperatures in the range 62−65 °C, indicating that helix 18 has little direct role in global thermal stability and that the thermal transitions at considerably lower temperatures involved in the on–off-rate alterations for NAD^+ indeed reflect local, reversible structural changes, probably within helix 18 itself.

Helix 18 and other nearby structures may therefore identify critical sites at which inhibitory ligands that have the capacity to distinguish between human and parasitic enzymes could be designed to bind. Such compounds have the potential to function as specific antiparasitic drugs. Figure 6 shows some of the details of the structures of helix 18 in Hs-SAHH, Tc-SAHH, and Pf-SAHH.

REFERENCES

1. Turner, M. A., Yang, X., Yin, D., Kuczera, K., Borchardt, R. T., and Howell, P. L. (2000) Structure and function of S-adenosylhomocysteine hydrolase. *Cell Biochem. Biophys. 33*, 101–125.
2. Yin, D., Yang, X., Yuan, C.-S., and Borchardt, R. T. (2000) in *Biomedical Chemistry: Applying Chemical Principles to the Understanding and Treatment of Disease* (Torrence, P. F., Ed.) pp 41–71, Wiley, New York.
3. Yang, X., and Borchardt, R. T. (2000) Overexpression, purification, and characterization of S-adenosylhomocysteine hydrolase from *Leishmania donovani*. *Arch. Biochem. Biophys. 383*, 272–280.
4. Creedon, K. A., Rathod, P. K., and Wellems, T. E. (1994) *Plasmodium falciparum* S-adenosylhomocysteine hydrolase. cDNA identification, predicted protein sequence, and expression in *Escherichia coli*. *J. Biol. Chem. 269*, 16364–16370.
5. Parker, N. B., Yang, X., Hanke, J., Mason, K. A., Schowen, R. L., Borchardt, R. T., and Yin, D. H. (2003) *Trypanosoma cruzi*: molecular cloning and characterization of the S-adenosylhomocysteine hydrolase. *Exp. Parasitol. 105*, 149–158.
6. Henderson, D. M., Hanson, S., Allen, T., Wilson, K., Coulter-Karis, D. E., Greenberg, M. L., Hershfield, M. S., and Ullman, B. (1992) Cloning of the gene encoding *Leishmania donovani* S-adenosylhomocysteine hydrolase, a potential target for antiparasitic chemotherapy. *Mol. Biochem. Parasitol. 53*, 169–183.
7. Whaun, J. M., Miura, G. A., Brown, N. D., Gordon, R. K., and Chiang, P. K. (1986) Antimalarial activity of neplanocin A with perturbations in the metabolism of purines, polyamines and S-adenosylmethionine. *J. Pharmacol. Exp. Ther. 236*, 277–283.
8. Seley, K. L., Schneller, S. W., De Clercq, E., Rattendi, D., Lane, S., Bacchi, C. J., and Korba, B. (1998) The importance of the 4′-hydroxyl hydrogen for the anti-trypanosomal and antiviral properties of (+)-5′-noraristeromycin and two 7-deaza analogues. *Bioorg. Med. Chem. 6*, 797–801.
9. Yang, X., Hu, Y., Yin, D. H., Turner, M. A., Wang, M., Borchardt, R. T., Howell, P. L., Kuczera, K., and Schowen, R. L. (2003) Catalytic strategy of S-adenosyl-L-homocysteine hydrolase: transition-state stabilization and the avoidance of abortive reactions. *Biochemistry 42*, 1900–1909.
10. Tanaka, N., Nakanishi, M., Kusakabe, Y., Shiraiwa, K., Yabe, S., Ito, Y., Kitade, Y., and Nakamura, K. T. (2004) Crystal structure of S-adenosyl-L-homocysteine hydrolase from the human malaria parasite *Plasmodium falciparum*. *J. Mol. Biol. 343*, 1007–1017.
11. Li, Q.-S., and Huang, W. (2004) The x-ray structure of S-adenosylhomocysteine hydrolase from *Trypanosoma cruzi* bound with Neplanocin A,PDB code 1XBE.
12. Ault-Riche, D. B., Yuan, C. S., and Borchardt, R. T. (1994) A single mutation at lysine 426 of human placental S-adenosylhomocysteine hydrolase inactivates the enzyme. *J. Biol. Chem. 269*, 31472–31478.
13. Komoto, J., Huang, Y., Gomi, T., Ogawa, H., Takata, Y., Fujioka, M., and Takusagawa, F. (2000) Effects of site-directed mutagenesis on structure and function of recombinant rat liver S-adenosylhomocysteine hydrolase. Crystal structure of D244E mutant enzyme. *J. Biol. Chem. 275*, 32147–32156.
14. Li, Q.-S., Cai, S., Borchardt, R. T., Fang, J., Kuczera, K., Middaugh, C. R., and Schowen, R. L. (2007) Comparative kinetics of cofactor association and dissociation for the human and trypanosomal S-adenosylhomocysteine hydrolases. 1. Basic features of the association and dissociation processes. *Biochemistry 46*, 5798–5809.
15. Yuan, C. S., Yeh, J., Liu, S., and Borchardt, R. T. (1993) Mechanism of inactivation of S-adenosylhomocysteine hydrolase by (Z)-4′,5′-didehydro-5′-deoxy-5′-fluoroadenosine. *J. Biol. Chem. 268*, 17030–17037.
16. Yuan, C. S., Ault-Riche, D. B., and Borchardt, R. T. (1996) Chemical modification and site-directed mutagenesis of cysteine residues in human placental S-adenosylhomocysteine hydrolase. *J. Biol. Chem. 271*, 28009–28016.
17. Gomi, T., Takata, Y., and Fujioka, M. (1989) Rat liver S-adenosylhomocysteinase. Spectrophotometric study of coenzyme binding. *Biochim. Biophys. Acta 994*, 172–179.
18. Kallberg, Y., Gustafsson, M., Persson, B., Thyberg, J., and Johansson, J. (2001) Prediction of amyloid fibril-forming proteins. *J. Biol. Chem. 276*, 12945–12950.
19. Elrod, P., Zhang, J., Yang, X., Yin, D., Hu, Y., Borchardt, R. T., and Schowen, R. L. (2002) Contributions of active site residues to the partial and overall catalytic activities of human S-adenosylhomocysteine hydrolase. *Biochemistry 41*, 8134–8142.
20. Facchiano, A. M., Colonna, G., and Ragone, R. (1998) Helix stabilizing factors and stabilization of thermophilic proteins: an X-ray based study. *Protein Eng. 11*, 753–760.
21. Marshall, S. A., Morgan, C. S., and Mayo, S. L. (2002) Electrostatics significantly affect the stability of designed homeodomain variants. *J. Mol. Biol. 316*, 189–199.
22. Richardson, J. S., and Richardson, D. C. (1988) Amino acid preferences for specific locations at the ends of alpha helices. *Science 240*, 1648–1652.

BI800175G